

Wade A. Meith,¹ Michael R. Hill,¹ and Tina L. Panontin²

Analytical and Experimental Study of Fracture in Bend Specimens Subjected to Local Compression

Reference: Meith, W. A., Panontin, T. L. , Hill, M. R., “Analytical and Experimental Study of Fracture in Bend Specimens Subjected to Local Compression,” *Fatigue and Fracture Mechanics: 33rd Volume, ASTM STP 1417*, W. G. Reuter and R. S. Piascik, Eds., American Society for Testing and Materials, West Conshohocken, PA, 2002.

Abstract: This study presents finite element simulations and fracture predictions for experimental conditions in a recent ASTM round-robin program on weld fracture toughness. The simulations include the effects of weld residual stress and residual stress alteration due to local compression of notched SE(B) specimens. Simulations are performed for a variety of material models and local compression details. Fracture is predicted using crack-tip stress and strain as inputs to both a local and a global prediction scheme. The local prediction is based on the RKR micromechanical model. The global prediction is based on obtaining a critical value of the J -integral, computed using a modified domain integral. Results predict that fracture toughness in the round robin was markedly reduced by local compression of the specimens. The amount of the reduction depends on the position of the compression platen relative to the notch-tip, but is largely independent of the amount of local compression applied. Available data from the round robin do not completely confirm the prediction results, but some of these data may have been influenced by warm pre-stressing during fatigue pre-cracking.

Keywords: Local compression, weld metal, residual stress, fracture toughness

Introduction

This study presents fracture predictions for welded and locally compressed fracture test coupons used in a recent ASTM round-robin testing program. Residual stresses in fracture test coupons removed from larger welded joints often promote preferential crack growth in some areas (tensile stress) while inhibiting growth others (compressive stress). This can create a curved crack front following fatigue pre-cracking, which may invalidate

¹ Graduate student and Assistant Professor, respectively, Department of Mechanical and Aeronautical Engineering, University of California, One Shields Avenue, Davis, CA 95616.

² Chief Engineer, NASA Ames Research Center, MS 213-4, Moffett Field, CA 94035-1000.

subsequent fracture measurement. The process of local compression has been used to alter residual stresses near the machined notch in fracture specimens, enabling a straighter pre-crack to be introduced [1]. Although the local compression process provides a straighter crack, it has been argued that it also reduces the fracture load, giving a lower apparent toughness than would be found in the same material free of residual stress [2]. Despite this drawback, the need for fracture measurements in weld metal has caused ASTM to draft a proposed Annex to ASTM E-1290 Standard Method for Crack-Tip Opening Displacement (CTOD) Fracture Toughness Measurement to allow for local compression when testing weld metals. A recent ASTM round-robin test program was initiated to demonstrate the suitability of the proposed Annex. This paper attempts to quantify the impact of local compression on the results of the test program.

The paper describes residual stress measurement, finite element modeling, and fracture prediction for the experimental conditions in the ASTM round robin. It reports the experimental determination of initial residual stresses in specimen blanks. It further describes simulation of local compression and fracture loading of the residual stress bearing specimens. Fracture is predicted using both a local and a global approach, each based on finite element predictions of crack-tip stress and strain. The local approach uses a critical stress and length scale. The global approach uses the crack driving force, as determined by a modified domain J -integral formulation which properly accounts for prior plastic work and residual stress. Parametric results are provided to investigate the sensitivity of the computations to the position of the locally compressed region, to the amount of local compression, and to the assumed material model. Preliminary round-robin fracture results provided by two participating laboratories are incorporated to calibrate fracture models and assess the modeling results.

Round-robin Test Program

The ASTM round-robin consisted of fabrication, local compression, fatigue pre-cracking, and fracture testing of SE(B) samples removed from a large-diameter, longitudinally-welded pipe. Local compression (LC) and pre-cracking were performed at room temperature while fracture testing was performed on the lower shelf (-196 C). Notched SE(B) specimens and un-notched specimen blanks were obtained by the authors and used in the present study to investigate the weld geometry, material properties, and to measure residual stresses. The authors did not perform fracture testing, but did obtain fracture test results from two laboratories that responded to a call for data. These laboratories provided detailed information on their laboratory procedures and also submitted fracture toughness results.

The welded pipe from which specimens were removed was fabricated from pressure vessel steel. The SE(B) specimens were removed from the pipe with the span dimension transverse to the weld, the crack growth direction along the weld, and the crack front sampling the entire weld thickness. A typical SE(B) specimen is shown in Figure 1. Material properties for the weld and parent materials were provided in the ASTM round-robin instructions for both ambient and lower-shelf temperatures. These properties are reported in the first four data columns of Table 1, and indicate that the weld and parent materials are low-hardening and closely matched. The last row of this table lists approximate Ramberg-Osgood hardening exponents found from the yield and ultimate strengths as suggested by Kirk and Wang [3]. The last four columns of Table 1 are

described below.

The two responding laboratories applied LC differently and reported different fracture toughness. Laboratory A applied LC simultaneously to both sides of the specimen, using 12.7 mm platens centered over the tip of the pre-crack starter notch, as shown in Figure 2(a). The center of the platen was located $0.43W$ from the front face of the specimen (i.e., $d/W = 0.43$ where d is the distance from the front face of the SE(B) to the center of the indentation). Laboratory B applied LC in two stages, compressing one side, then the other as shown in Figure 2(b) and (c). Laboratory B used a 12.7 mm platen centered at $d/W = 0.65$. Laboratory A performed fracture testing for specimens with 0%, 1%, and 2% LC. Laboratory B performed fracture testing for 1% LC. Fracture test results are summarized in Figure 3 and show a disparity in measured toughness at 1% LC.

Residual Stress Determination

In order to assess the influence of pre-existing weld residual stress on the round-robin results, residual stress was measured in an un-notched specimen blank. Relative to the fracture specimen, the opening mode residual stress was measured as a function of the through-thickness position (i.e., relative to the coordinates in Figure 1, the yy -component of residual stress was measured as a function of z). Since chemical etching revealed no evidence of a weld start-stop cycle in the specimen blank, residual stress was assumed to be invariant of the position along the weld (x -direction). That is, etching indicated a

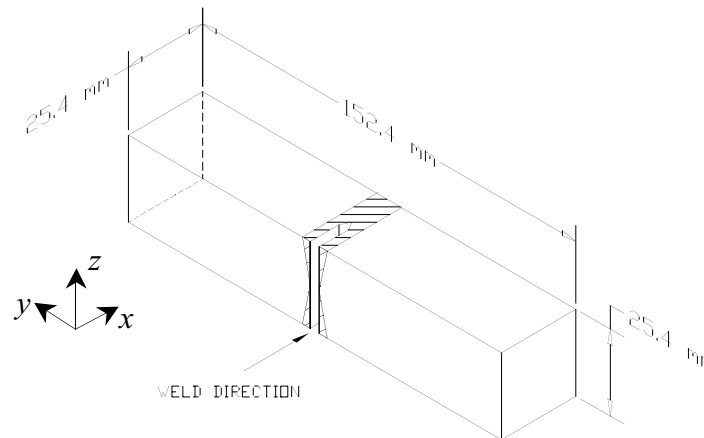


Figure 1 – Typical SE(B) specimen with coordinate directions assumed

Table 1 – Mechanical properties of weld and parent materials

Source	Round-robin instructions				Hardness-adjusted		Low hardening	
	Weld		Parent		Parent		Weld	
Temp (C)	21	-196	21	-196	21	-196	21	-196
S_y (MPa)	548	888	514	848	484	785	548	888
S_u (MPa)	593	989	593	960	524	874	—	—
E (GPa)	206	218	206	218	206	218	206	218
ν	0.3	0.3	0.3	0.3	0.3	0.3	0.3	0.3
n	25.2	20.4	16.8	18.5	25.2	20.4	--	--

continuous weld process was used and continuous welding induces residual stress largely invariant of position along the weld [4]. The compliance method was used to estimate the residual stress [5, 6]. Strain gages were attached on the upper and lower weld surfaces and the specimen blank was sliced incrementally in the z -direction using wire electric discharge machining, as shown in Figure 4. Strain released at the top and bottom gages was gathered as a function of z -direction depth of cut and these data used in a finite-element-based back-calculation scheme to determine residual stress in the specimen blank prior to slicing. The resulting residual stress distribution will be used in finite

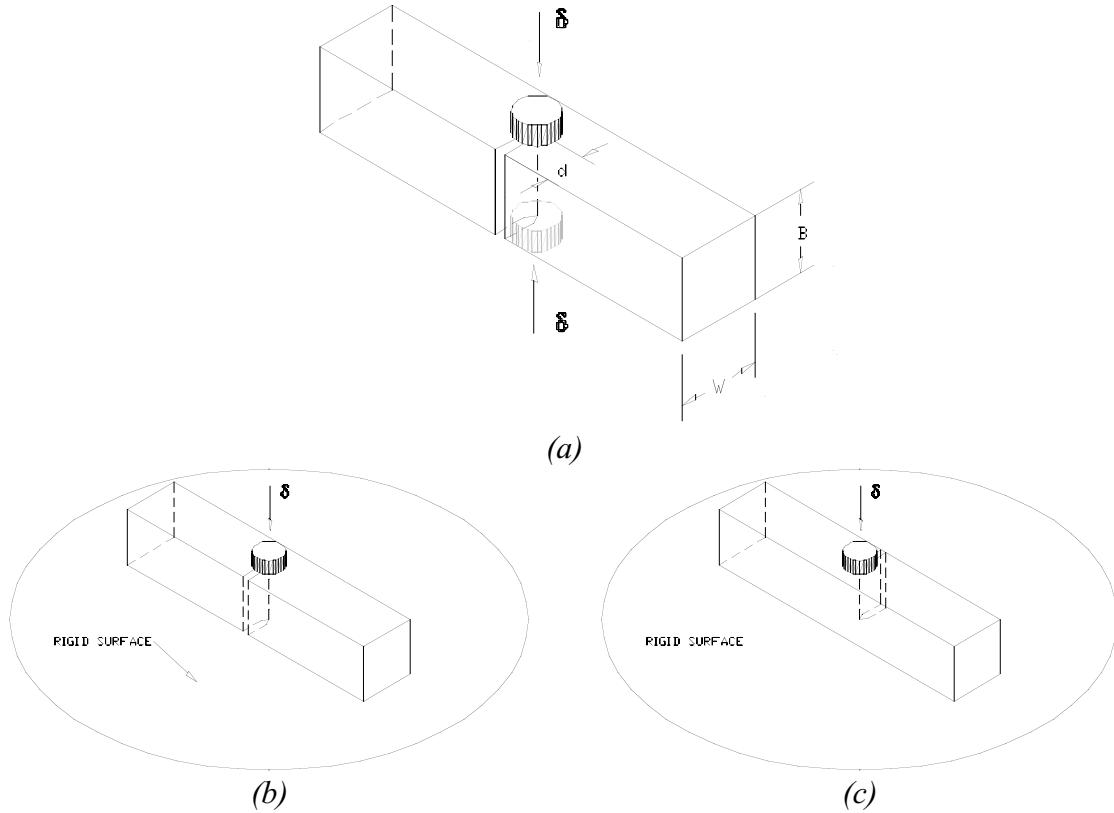


Figure 2 – Application of local compression: (a) Laboratory A; (b) and (c) Laboratory B

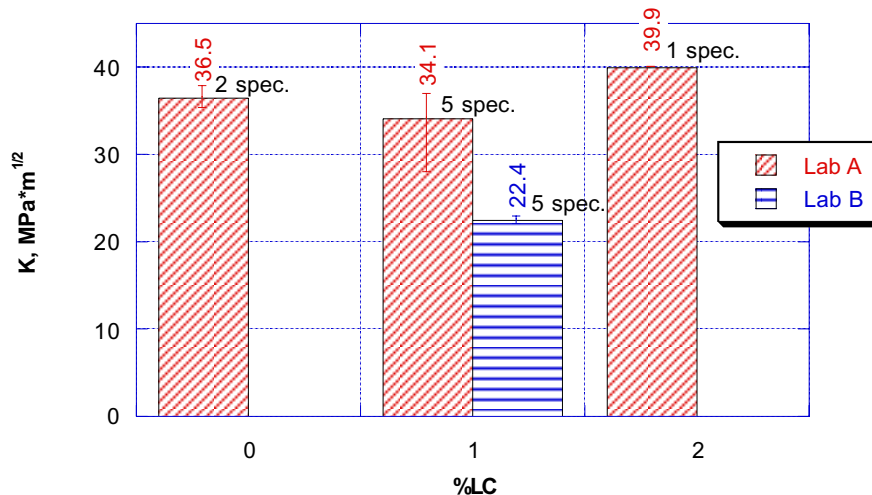


Figure 3 – Fracture toughness obtained by both laboratories for various amounts of LC

element simulation of the round-robin specimens as described below.

Fracture Prediction

Fracture prediction for specimens in the round robin study requires a significant amount of information and analysis. Fracture in the specimens occurred due to the combined action of applied loading and residual stress. The residual stress in locally compressed specimens is complex, but has been previously predicted by directly simulating the elastic-plastic compression process [2]. The material response during LC depends on the pre-existing weld residual stress. So, the crack-tip conditions that initiate fracture depend on weld residual stress, residual stress due to LC, and stresses due to applied three-point bend loading. In the present study, the finite element method is used to account for these three contributions to the crack-tip state. The crack-tip conditions found over a range of applied load are then used to predict the fracture load during three-point bending.

Fracture models

Fracture is predicted following two distinct approaches. The need for two approaches lies in uncertainty regarding the correct methodology for lower-shelf fracture prediction under varying constraint conditions. Lower-shelf behavior is thought to depend on opening stress and be invariant to the state of strain [7]. However, experimental evidence on the lower-shelf suggests that fracture is independent of constraint [8]. These two points of view lead to a contradiction since different constraint implies different crack-tip stresses at the same value of driving force. The contradiction is important in the present study because previous finite element modeling of LC indicated that the process markedly increases constraint in three-point bend specimens [2]. Therefore, the present study predicts fracture in two ways, one dependent on and another independent of constraint.

The constraint-dependent fracture model is a local approach based on achieving a critical level of opening stress over a fixed length scale. Initiation of cleavage fracture in mild steels can be predicted using the RKR micromechanical model [7]. This relatively simple model predicts fracture when the opening stress, σ_{yy} , ahead of the crack-tip exceeds a fracture stress, σ^* , over a microstructurally relevant distance, l^* . In applying

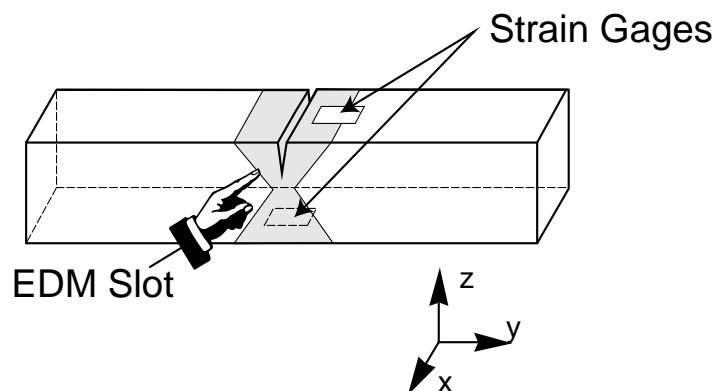


Figure 4 – Strain gage locations and slot orientation for residual stress determination.

this model, one monitors the progress of the opening stress ahead of the crack-tip due to residual and applied loading. Once the RKR criterion is satisfied, the associated applied load and deformation can be found from the FEM results and can be used to derive an *apparent* toughness comparable to laboratory results. The parameters in the RKR model are typically found through laboratory testing for a given material and reported ranges for steels are 2 to 5 grain diameters for l^* , and 2 to 4 times the yield strength for σ^* [7].

The constraint independent fracture model is based on achieving a critical level of the J -integral at some point along the crack front. The domain integral technique is used to compute J from finite element predictions of stress, strain, and deformation in domains surrounding the crack tip [9]. The current analysis conditions require special care when computing the domain integral because residual stress and plastic work of LC cause path dependent values of J . Recent research has provided a methodology to obtain contour independent values of J for these conditions [10, 11]. A computer program was written to employ these methods for three dimensional finite element results from the present analyses. Since residual stress due to welding and LC varies along the crack front, the maximum value of J along the front is assumed to control fracture. To highlight the fact that the values of J presented in this study are computed using the domain integral, and therefore include the combined effects of residual stress and applied loading, the results will be referred to as J_{DI} .

The fracture prediction models are calibrated from the test results for non-locally compressed specimens provided by Laboratory A and shown in Figure 3. That is, we impose residual stress and applied three-point bending on a finite element model of the SE(B) specimen (but do not simulate local compression). The three-point bend load for calibration is found from the model geometry, the average toughness found by Lab A ($K_{cal} = 36.5 \text{ MPa}\sqrt{\text{m}}$), and the stress intensity factor solution in ASTM E 1290, and is $P_{cal} = 13.6 \text{ kN}$. When the model is loaded to this force, the finite element results are used to calibrate the RKR and J_{DI} models. The maximum value of J_{DI} found along the crack front is taken to be the level of J controlling fracture, J_{cal} . Since the RKR model has two fracture parameters and we use only a single calibration condition, we assume two different values of σ^* and identify l^* for each as the largest distance ahead of the crack tip where $\sigma_{yy} = \sigma^*$. The two values assumed for σ^* are $2 S_y$ and $2.5 S_y$, and the corresponding predictors are referred to as RKR₁ and RKR₂. As will be shown, the small range of assumed fracture stress produces length scales that differ by a factor of 2 and therefore predict somewhat different fracture loads in the locally compressed specimens. Given these three calibrated fracture models, we can predict fracture for the specimens with the range of LC shown in Figure 3.

Finite element modeling

General - Elastic-plastic finite element computation is used to simulate the response the SE(B) to both applied and residual stresses simultaneously. The finite element solutions employ a non-linear, finite strain formulation. Plasticity is assumed to follow isotropic, incremental J_2 flow theory with a piece-wise linear Cauchy-stress logarithmic-strain curve obtained from power-law fits derived from the material strengths given in the round-robin instructions. The commercial code ABAQUS is used to perform the analyses [12]. Mesh refinement in the crack-tip region was chosen to assure that stress and strain

are accurately captured in the near-tip region. Time stepping in the analysis provides a means to capture the developing crack-tip state with increasing applied load.

The three-dimensional model of the SE(B) is shown in Figure 5. The model is composed of eight-node, hexahedral elements with reduced integration. The model dimensions are as shown in Figure 1 with a crack length of $a/W = 0.5$. Quarter symmetry was used, with one symmetry plane halving the span of the specimen, and another halving the thickness. To simulate three-point bending, nodal constraints in the x -direction were imposed at the roller location and displacement applied in the negative x -direction on the span symmetry plane. This load was split between two sets of nodes to reduce the tendency for strain localization at the load point. The mesh has an initially blunted crack tip with radius of 4.82μ to enhance convergence. The mesh has ten layers of elements through the model thickness with a geometric progression of element thickness such that midplane elements are ten times thicker than those at the free surface.

Weld residual stress - Pre-existing weld residual stress in the SE(B) specimens is included in the finite element computations using eigenstrain. Eigenstrain is a spatially varying, second order tensor that represents the combination of all inelastic, incompatible strains set up during processing of a material [13]. In welding, the eigenstrain is a combination of thermal, plastic, and transformation strains. The eigenstrain field is defined with reference to elastic deformation of the structure, and reproduces the entire RS state when the material behavior is elastic. For a particular process the eigenstrain field is a tensor with spatial dependence, and can be found experimentally [14] or by modeling [15].

The use of an eigenstrain distribution in modeling offers several advantages for further analysis. First, the residual stress present can be determined by imposing the eigenstrain distribution in a linear elastic finite element model of the geometry. (Note that residual stresses, by their nature, do not result in active yielding, and a valid eigenstrain field must impose stresses that satisfy the yield criterion). Although an eigenstrain analysis is complicated by the spatial variation of each component of the eigenstrain tensor, a general-purpose finite element program can be used to produce the RS field. Further, when the eigenstrain field is known, the entire, full-field, triaxial RS state is known at every point within the structure.

When the eigenstrain field is known for the unflawed structure, the analysis of a flawed structure can be performed. The addition of a crack introduces new surfaces, and the RS state in the flawed body depends on these surfaces. If the structure is linear elastic, the state is found simply by modeling the traction-free surfaces. In non-linear materials, crack-tip yielding must be allowed when introducing the flaw. To handle this situation, the eigenstrain distribution is first imposed in the body with crack-face nodes restrained, and the equilibrium RS state found (this step is elastic). Then, the crack-face nodes are released in succession, so that the crack gradually extends from the free surface to simulate fatigue (this step can be elastic-plastic). The rate at which the crack is extended will have a bearing on the crack-tip fields, and one must ensure that the opening is gradual enough (e.g., so subsequent fracture analysis is not adversely affected). When properly executed, this process redistributes the original RS field, allowing for crack-tip yielding, and resulting in a flawed RS bearing structure.

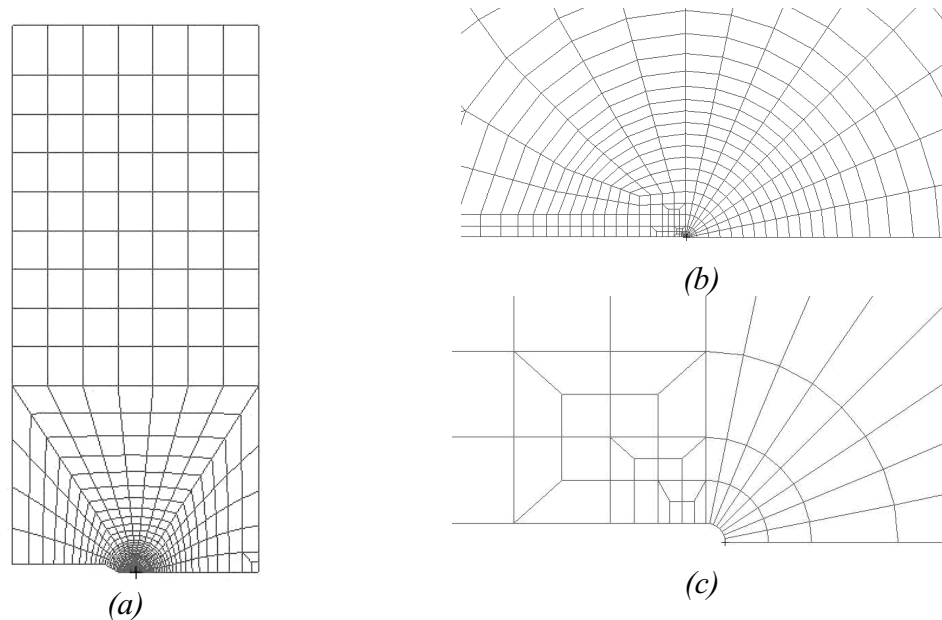


Figure 5 – Finite element mesh: (a) full mesh, (b) and (c) detail of crack tip

The specific eigenstrain distribution used in this work was derived from residual stress determined experimentally. As will be shown later, the opening residual stresses were found to closely resemble a sinusoidal variation through the weld joint thickness. The stress measurements were made only on the weld centerline which coincides with the span symmetry plane in the SE(B) specimens. In order to distribute the stresses throughout the SE(B) model it was assumed that the residual stresses are a maximum on the weld centerline and that they decay smoothly with distance from the weld centerline. Previous work on weld residual stresses used a tensor-product representation to distribute eigenstrain spatially in the transverse and through-thickness weld directions [16]. We will modify this distribution to match the experimentally determined stress. Since the particular eigenstrain distribution depends on the residual stress results, the eigenstrain distribution is described below.

Local compression - The application of LC is modeled in three distinct steps. The first step drives a mathematically defined rigid surface, which represents the compression platen, into the surface of the SE(B) using contact procedures. The second step removes enough of this displacement so that the third step will be entirely elastic. The third step then completely removes the contact relation between the rigid surface and the SE(B). Because the finite element model employs symmetry about the specimen thickness, the LC simulation most closely reflects the procedures of Laboratory A. Various amounts of local compression are simulated. The rigid surface displaces in the thickness direction of the specimen to compress the surface and leave a final reduction in thickness of 0.5%, 1% or 2% after removal of the rigid surface from the model.

In actual testing, LC is followed by fatigue pre-cracking prior to loading to fracture. To simulate the pre-cracking process, crack-face nodes within $0.07W$ behind the crack-tip in the SE(B) mesh are restrained during the compression process and are released after compression loads are removed. This strategy leaves a plastic zone due to residual stress remaining after LC, but no attempt is made to account for plasticity or other effects related to fatigue pre-cracking loads. Simulation of a locally compressed specimen, then,

consists of seven steps: 1) find residual stress (equilibrium) in the presence of eigenstrain due to welding, 2) apply LC displacements, 3) reduce LC displacements, 4) remove the platen rigid surface from the model, 5) release crack-face tractions to simulate pre-cracking, 6) reduce the ambient temperature to change material properties, and 7) apply three-point bend loads to fracture.

Material models

Round robin material information and hardness tests performed on specimen blanks were examined to decide the best method for modeling the welded specimens. Test specimens were fracture tested at low temperature and hence exhibited low toughness and small scale yielding. Since the crack-tip plastic zone was likely small enough to be entirely in the weld metal, a homogeneous material model is a viable option. However, LC causes plastic deformation outside the weld (at room temperature) and this suggests that a bimaterial model may be a better approach, with one flow curve for the weld and one for the base metal. Although the strengths in Table 1 suggest that the weld and parent metal are well-matched, a hardness traverse conducted on a specimen blank suggested that the weld metal was considerably stronger than the parent metal, with hardness in the weld bead averaging 94 HRB and in the parent metal averaging 89.5 HRB. Conversion from these hardness values to ultimate strengths (by converting to Brinnell hardness and multiplying the result by 0.5) suggests that the parent metal strength is about 89% of that in the weld metal.

Because the hardness results suggest a contradiction with the strengths shown in the first four data columns of Table 1, three material combinations were investigated in this study. The first material model uses a single, power-law hardening flow curve for each temperature corresponding to the weld metal data shown in Table 1. The second material model uses two flow curves for each temperature, one for the parent and one for the base metal. The parent flow curves were found by multiplying the weld metal power-law flow curves by the ratio of the hardness-indicated strengths (0.89). These flow curves are shown in Figure 6. The weld region of the SE(B) was assumed to be 12.7 mm wide which followed from the hardness traverse and from physical measurements on a polished and chemically etched specimen blank. In order to assess the sensitivity of the modeling to the amount of hardening assumed, an additional material model was considered. The power-law hardening flow curves are an approximation that may not reflect the actual near-yield behavior of the material (e.g., the presence of a sharp yield point would not be accounted for). To assess the sensitivity of the models to initial hardening, a nearly perfectly plastic flow curve was also used. For this model, the SE(B) was assumed to be homogeneous, with yield strength equal to the weld material as reported in Table 1. A small post-yield tangent modulus (0.05% S_y) was added to enhance convergence of the finite element computations.

Again, the objective of the current study is to model the experimental conditions of the round-robin program. Since different experimental approaches were pursued, a parametric study was performed. The parameters related to LC are the location of the compression platen and the amount of compression. The three material models described above were also included as parameters. Table 2 shows the computations performed in the current study. The platen position, amount of compression, and material model were varied as shown.

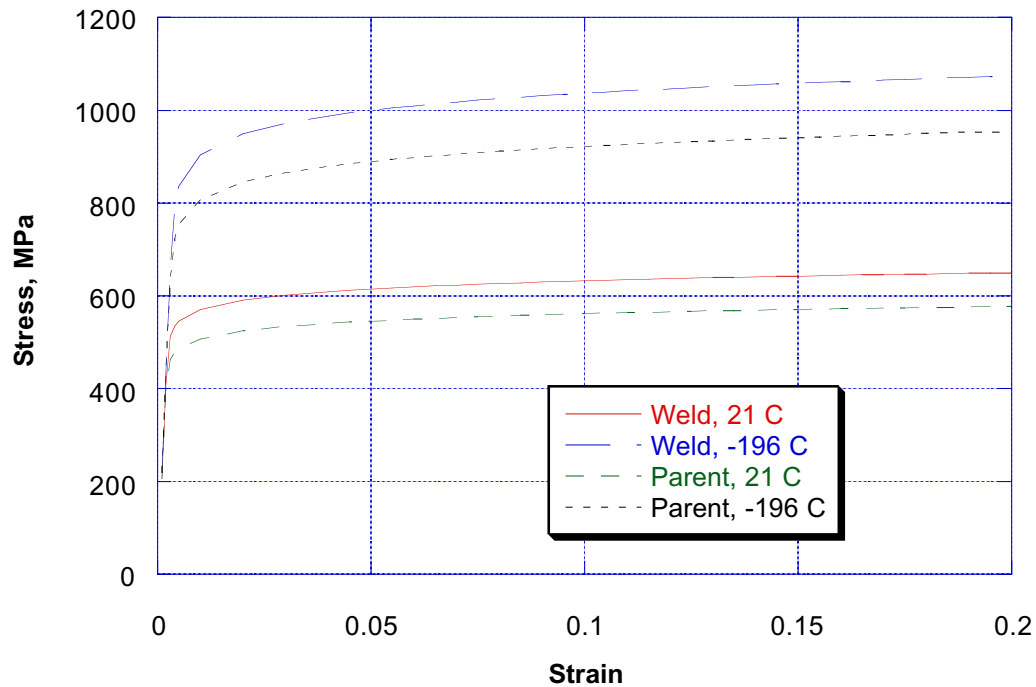


Figure 6 – Ramberg-Osgood material curves for the weld and parent materials at both temperatures

Table 2 – Seven simulations for various combinations of the platen location, amount of LC, and material model reported in this study

Platen Center (d/W)	% LC	Material Model		
		All Weld	Bimaterial	Low Hardening
0.43	0.5	X		
	1.0	X	X	X
	2.0	X		
0.5	1.0	X		
0.57	1.0	X		

Results

Residual stress distribution

Residual stress found using the compliance method is shown in Figure 7, normalized by the weld metal yield strength. Also shown in the figure are the results of an elastic eigenstrain analysis described below. The experimental results are in contrast to some typical distributions of residual stress that often show yield-level tension on the surfaces and compression in the interior. However, the difference between this distribution and typical results is likely due to residual stress redistribution that occurred when the specimen blank was removed from the larger welded pipe. The magnitude of the residual stress is quite low throughout the specimen in comparison to the yield strength of the material. Although the residual stresses are relatively small, they can still affect the ability to obtain a straight-fronted fatigue pre-crack in the fracture specimens.

Assuming coordinates centered in the SE(B) specimen, and oriented as indicated in Figure 1, the eigenstrain distribution is given by

$$\begin{aligned}
 \varepsilon_{xy}^* &= \varepsilon_{yz}^* = \varepsilon_{xz}^* = \varepsilon_{zz}^* = 0 \\
 \varepsilon_{xx}^* &= -\nu \varepsilon_{yy}^* / (1 - \nu) \\
 \varepsilon_{yy}^* &= -2.8 \cdot 10^{-4} f(y)g(z) \\
 f(y) &= \begin{cases} 0.5 * (1 + \cos(2\pi y / t)) & y < t/2 \\ 0 & y \geq t/2 \end{cases} \\
 g(z) &= \cos(2\pi z / t)
 \end{aligned} \tag{1}$$

where, ε_{ij}^* are the components of the eigenstrain tensor, ν is Poisson's ratio, and t is the thickness of the welded joint (25.4 mm). This eigenstrain distribution imposes an opening stress distribution similar to that found experimentally, when imposed in an un-notched specimen geometry. Figure 7 compares the results of an elastic finite element analysis using the eigenstrain given by Equation (1) with the experimentally determined stress. There are four curves for the eigenstrain model, with $y/t = 0$ corresponding to the experimental slotting location. The peak levels of residual stress are in agreement. The eigenstrain results further show how the residual stress magnitude decreases with distance from the center of the weld (i.e., increasing values of y/t).

Fracture model calibration

Calibration was performed by simulating a non-locally compressed, weld residual stress bearing SE(B) and using the resulting crack-tip region stresses and strains to satisfy the failure models at a load corresponding to K_{cal} . The material response at the crack tip is slightly different for each of the three material models, so each is calibrated separately. Opening stress for the calibration loading condition and the all weld material model is shown in Figure 8 (the three other curves are described below). The opening stress reaches $2.5 S_y$ at $x/W = 0.0018$, so the length scale for RKR_1 is 46.9μ . The length scale for RKR_2 is similarly found to be 111μ . Simulations and analyses for the other material models provide the calibration parameters reported in Table 3. The J_{DI} model is calibrated by computing J at the calibration loading condition and taking the maximum value of J_{DI} along the crack front. The J_{DI} calibrations are given for each material model in Table 3.

Fracture prediction

Fracture predictions for the all weld material model with the platen positioned over the notch-tip are shown in Figure 9. Results are presented in terms of the apparent toughness, which is computed from the load and geometry using the stress-intensity factor solution in ASTM E-399. The apparent toughness is normalized by the stress intensity factor used in calibrating the fracture models, $K_{cal} = 36.5 \text{ MPa}\sqrt{\text{m}}$. The fracture models predict that LC should reduce toughness 45 to 65% relative to the un-compressed specimens. The exact predictions depend more strongly on the fracture model assumed than on the amount of LC imposed. The differences among the fracture models result from constraint differences caused by LC. The opening stress distributions for 1% LC

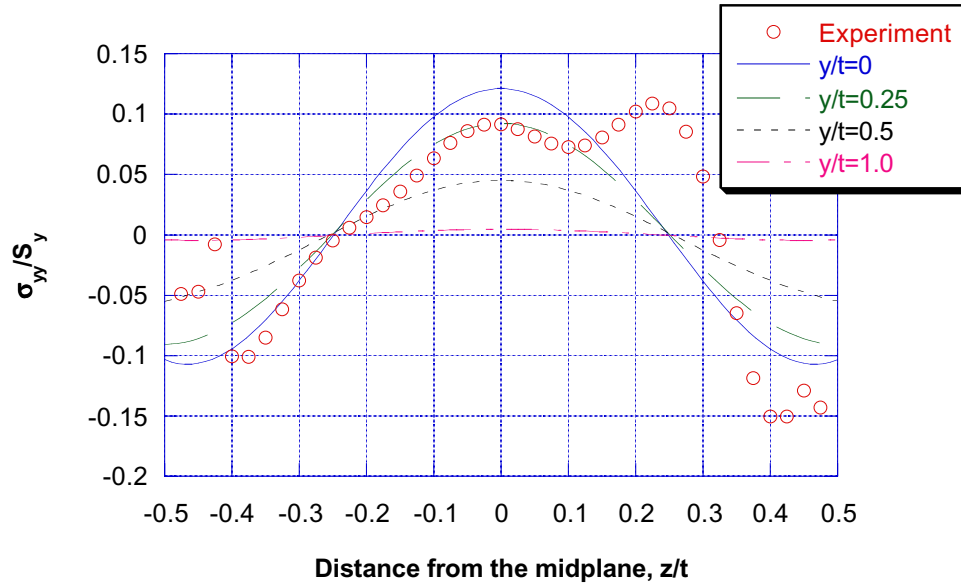


Figure 7 – Comparison of residual stress from experiment with that created in the specimen blank when loaded by the eigenstrain field given by Equation (1)

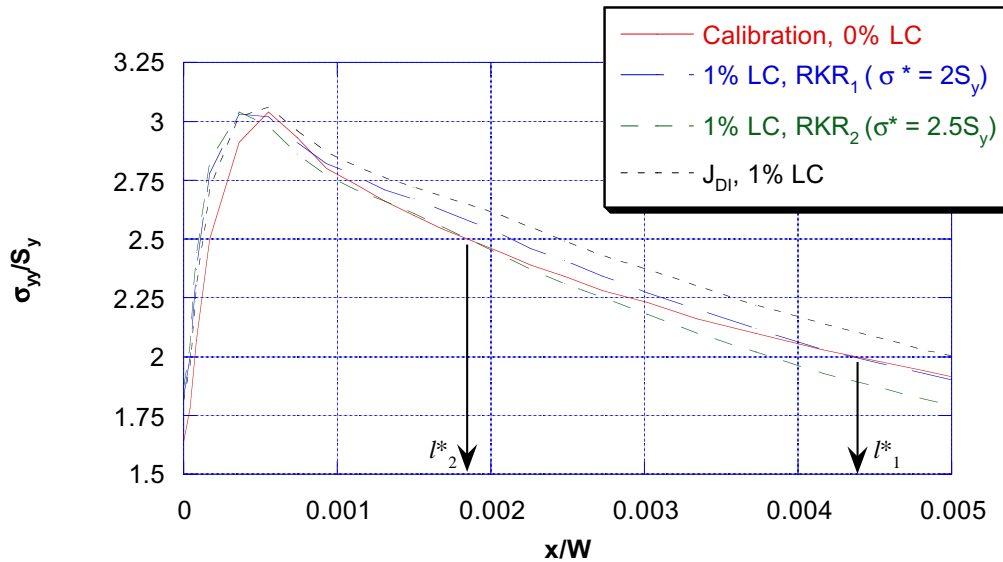


Figure 8 – Midplane opening stress ahead of the crack-tip for the all weld model at the calibration loading and at failure for 1% LC and $d/W = 0.43$ as defined by the three fracture models

Table 3 – Calibration values

Material Model	J_{cal} , kJ/m^2	l^* ($\sigma^* = 2S_y$), μ	l^* ($\sigma^* = 2.5S_y$), μ
All Weld Material	7.09	111	46.9
Bimaterial	7.15	111	46.9
No Hardening	7.14	120	48.0

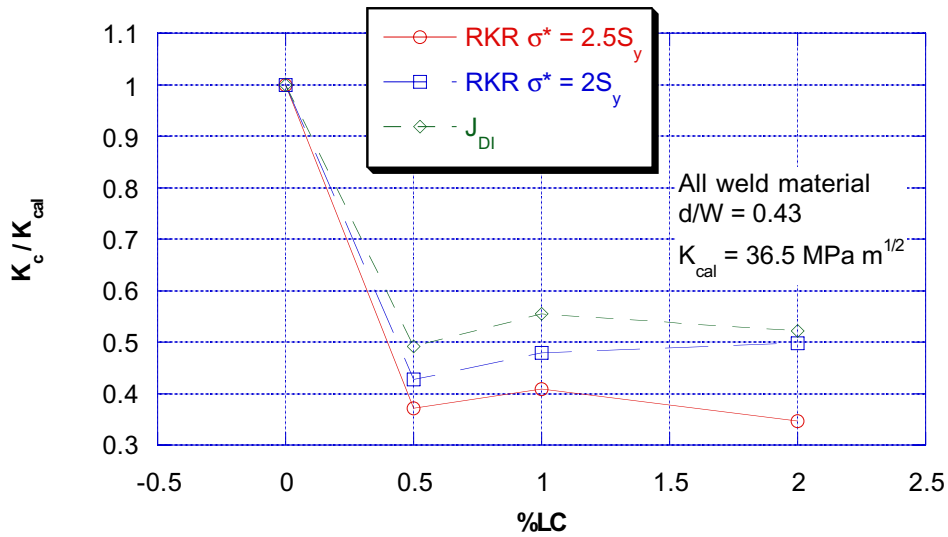


Figure 9 – Apparent toughness versus % LC for all weld material model, platen centered at $d/W = 0.43$

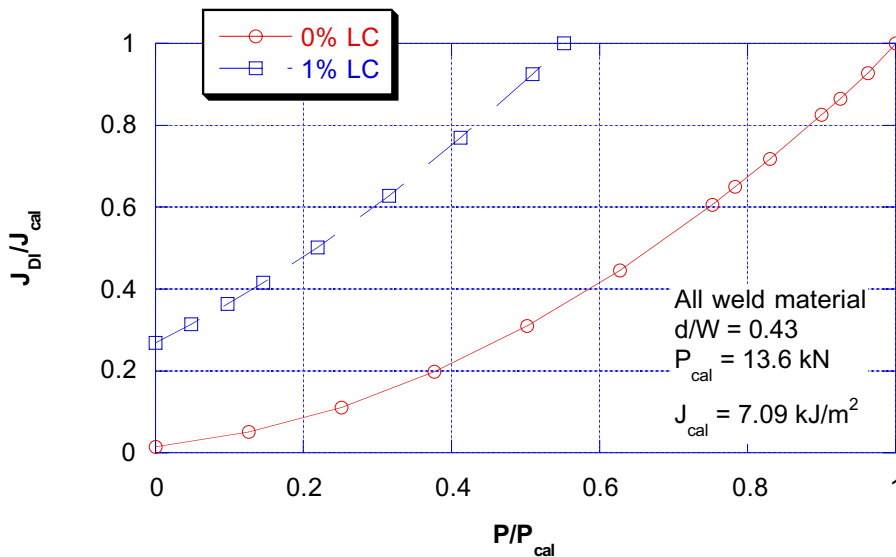


Figure 10 – Comparison J_{DI} versus applied load for the all weld material model at different amounts of LC

and the all weld material model are shown with the calibration condition in Figure 8. The three curves show the opening stress at the fracture load predicted by the corresponding model. The J_{DI} curve shows that the same J results in higher opening stresses in the 1% LC model, which indicates higher constraint. The two RKR prediction curves are lower than the J_{DI} curve because they are sensitive to the LC-imposed constraint. The RKR predictors therefore indicate a larger effect of LC.

The impact of LC on crack driving force can be observed by examining the development of J_{DI} with applied load. LC causes a non-zero driving force at zero applied

load. This is demonstrated in Figure 10, which plots J_{DI} versus the applied load for un-compressed and 1% compressed models. The large value of J_{DI} at zero applied load in the LC model serves to decrease the predicted fracture load and therefore the apparent toughness. The figure further indicates that the residual stress state in the un-compressed SE(B) produces only a small J_{DI} at zero applied load. The small magnitude is due to the fact that the residual opening stresses are small and nearly equilibrate along the crack front.

Figure 11 illustrates the influence of platen location on apparent toughness. The specific locations of the platen center correspond to the starter notch tip, the pre-crack tip, and a position ahead of the pre-crack tip. The results suggest that moving the platen center toward the back face reduces apparent toughness. Since the RKR and J_{DI} predictions converge when the platen is further over the ligament ($d/W = 0.57$) the effect at that position is mainly due to the contribution of residual stress imposed by LC to the crack driving force. The smallest effect on apparent toughness occurs when the center of the compression platen is between the pre-crack tip and the front face.

Figure 12 shows the influence of the material model on the apparent toughness for 1% compression with the platen centered on the notch tip. These results indicate a significant sensitivity to the assumed flow curve. The difference between the low hardening and all weld models suggests that strain hardening increases the effect of LC. The bimaterial model predicts a larger influence of LC than either of the two homogeneous material models. The results presented in Figure 12 show that accurate determination of the weld and base metal flow curves is important in predicting the influence of LC on apparent toughness.

To first order, the influence of LC on apparent toughness predicted for the SE(B) depends on the J_{DI} at zero load following compression. Table 4 shows this quantity, normalized by J_{cal} , for each analysis condition, where a larger value suggests a larger LC-induced toughness change. The driving force of residual stress left by LC increases with d/W which agrees with the trends in Figure 11. J_{DI} at zero load also suggests the same dependence of the material model on apparent toughness displayed in Figure 12.

Discussion

Comparison of the laboratory toughness measurements shown in Figure 3 with the model predictions suggests the models over-predict the effect of LC. The all weld, J_{DI} prediction trend is shown with the experimental data in Figure 13. While the data from Lab B compare favorably with the prediction at 1% LC, the data from Lab A do not. The test records from Lab A and B indicate that the pre-cracking loads differed significantly, producing final ΔK values of approximately $19 \text{ MPa}\sqrt{\text{m}}$ and $11 \text{ MPa}\sqrt{\text{m}}$, respectively, at $R = 0.1$. It is suspected that the elevated pre-crack levels used by Lab A led to warm pre-stressing and elevated toughness. The simulations suggest that pre-cracking loads in compressed specimens are superimposed on a positive residual driving force left by LC, therefore producing an even greater warm pre-stress effect than indicated by the applied loading. Additional tests are planned by Lab A to provide specimens pre-cracked at lower levels and obtain toughness measurements at 0% and 1% LC.

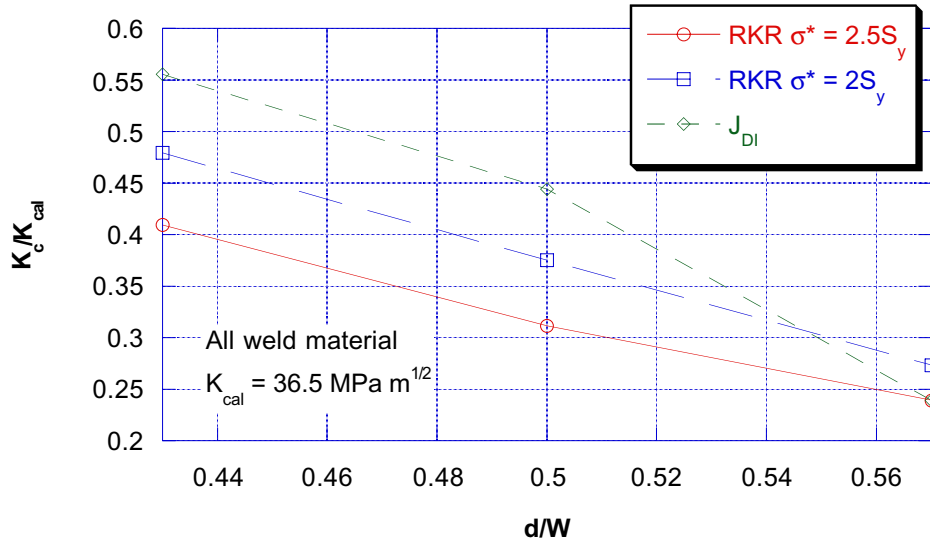


Figure 11 – Apparent toughness vs. platen location for the all-weld material model

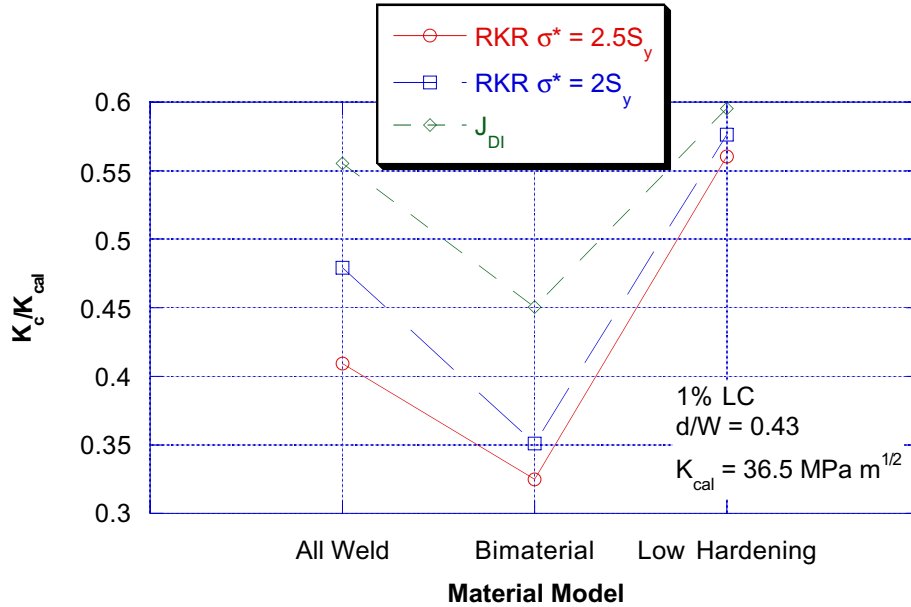


Figure 12 – Apparent toughness versus material model, 1% compressed and $d/W = 0.43$

Table 4 – J_{DI} at zero load normalized by J_{cal} for all seven cases analyzed ($J_{cal} = 7.09 \text{kJ/m}^2$)

Platen Center (d/W)	% LC	Material Model		
		All Weld	Bimaterial	Low Hardening
0.43	0.5	0.33		
	1.0	0.27	0.38	0.23
	2.0	0.30		
0.5	1.0	0.38		
0.57	1.0	0.62		

Although local compression is predicted to reduce toughness, the necessity of a straight pre-crack may require its use. The simulations provide some sensitivity information for local compression that can allow improved experiment design. The

simulations suggest that the amount of local compression is not a significant factor influencing the apparent toughness. They further suggest that positioning the compression platen toward the front face, rather than over the ligament, reduces the effect of LC on apparent toughness. The results also suggest that the material model is an important factor in predicting the impact of LC on apparent toughness. Finally, the results suggest that the mechanisms of failure will have an impact on the effect of LC. In this study, lower-shelf toughness may be best predicted by J_{DI} . If the tests were performed in the transition region, the RKR fracture model may be the better predictor because of its sensitivity to constraint. The failure mechanism is important, since the RKR predictions suggest a larger effect of LC.

Acknowledgements

The authors are indebted to their colleagues from Laboratories A and B, who submitted their round-robin data and answered many questions.

References

- [1] Towers, O. L. and Dawes, M. G., "Welding Institute Research On The Fatigue Precracking Of Fracture Toughness Specimens," *Elastic-Plastic Fracture Test Methods: The User's Experience*, ASTM STP 856, ASTM, Philadelphia, PA, 1985, pp. 23-46.
- [2] Hill, M. R. and Panontin, T. L., "Effect of Residual Stress on Brittle Fracture Testing," *Fatigue and Fracture Mechanics: 29th Volume*, ASTM STP 1332, T. L. Panontin and S. D. Sheppard, Eds., ASTM, West Conshohocken, PA, 1999, pp. 154-175.
- [3] Kirk, M. T. and Wang, Y.-Y., "Wide Range CTOD Estimation Formulae for SE(B) specimens," *Fracture Mechanics: 26th Volume*, ASTM STP 1256, W. G. Reuter, J. H. Underwood and J. C. Newman, Eds., American Society for Testing and Materials, Philadelphia, 1995, pp. 126-141.

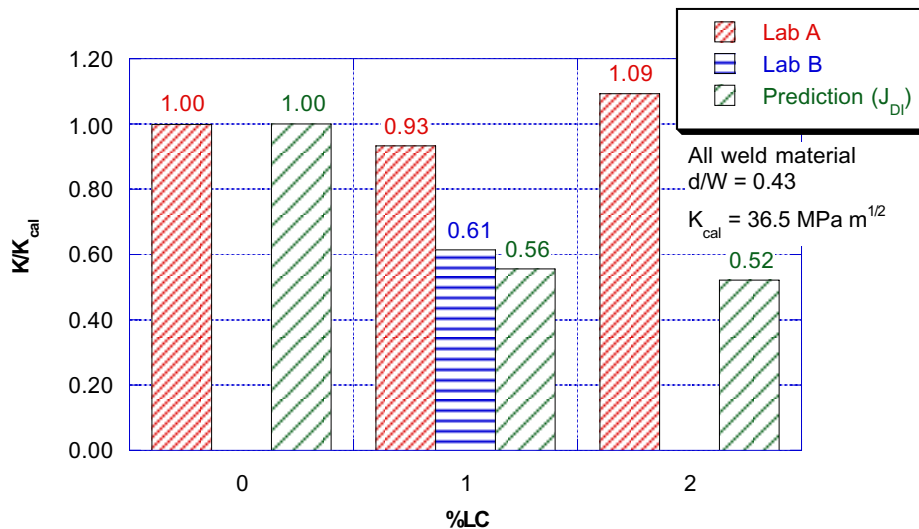


Figure 13 – Comparison of round robin experimental data with J_{DI} predictions

- [4] Masabuchi, K., *Analysis of Welded Structures: Residual Stresses, Distortion, and Their Consequences*, Pergamon Press, New York, 1980.
- [5] Prime, M. B., "Residual stress measurement by successive extension of a slot: The crack compliance method," *Applied Mechanics Reviews*, Vol. 52, No. 2, 1999, pp. 75-96.
- [6] Cheng, W. and Finnie, I., "Measurement of residual stress distributions near the toe of an attachment welded on a plate using the crack compliance method," *Engineering Fracture Mechanics*, Vol. 46, No. 1, 1993, pp. 79-91.
- [7] Ritchie, R. O., Server, W. L. and Wullarert, R. A., "Critical Fracture Stress and Fracture Strain Models for the Prediction of Lower and Upper Shelf Toughness in Nuclear Pressure Vessel Steels," *Metallurgical Transactions*, Vol. 10A, 1978, pp. 1557-1570.
- [8] Joyce, J. A., "J-Resistance Curve Testing of Short Crack Bend Specimens Using Unloading Compliance," *Fracture Mechanics: Twenty-Second Symposium (Volume I)*, ASTM STP 1131, American Society for Testing and Materials, Philadelphia, PA, 1992, pp. 904-924.
- [9] Carpenter, W. C., Read, D. T. and Dodds, R. H., "Comparison of several path independent integrals including plasticity effects," *International Journal of Fracture*, Vol. 31, 1986, pp. 303-323.
- [10] Lei, Y., O'Dowd, N. P. and Webster, G. A., "Fracture Mechanics analysis of a crack in a residual stress field," *International Journal of Fracture*, Vol. 0, 2000, pp. 1-22.
- [11] Matos, C. G. and Dodds, R. H. J., "Modeling the effects of residual stresses on defects in welds of steel frame connections," *Engineering Structures*, Vol. 22, 2000, pp. 1103-1120.
- [12] *ABAQUS/Standard, Version 5.8*, Hibbitt, Karlsson, and Sorenson, Inc., Providence, RI, 1999.
- [13] Mura, T., *Micromechanics of Defects in Solids*, M. Nijhoff, Dordrecht, Netherlands, 1987.
- [14] Hill, M. R., "Determination of Residual Stress Based on the Estimation of Eigenstrain," Doctoral Thesis, Stanford University, 1996.
- [15] Goldak, J. A. and Patel, B., "Computational Weld Mechanics," *Advanced Joining of Materials (AGARD CP-398)*, 1985, pp. 1-1 - 1-32.
- [16] Hill, M. R. and Nelson, D. V., "Determining residual stress through the thickness of a welded plate," *PVP*, ASME, New York, NY, 1996, pp. 29-36.